

Enhanced Lidov–Kozai migration and the formation of the transiting giant planet WD 1856+534 b

Christopher E. O’Connor^{1*}, Bin Liu¹, and Dong Lai^{1,2}

¹*Cornell Center for Astrophysics and Planetary Science, Department of Astronomy, Cornell University, Ithaca, NY 14853, U.S.A.*

²*Tsung-Dao Lee Institute, Shanghai Jiao Tong University, Shanghai 200240, China*

Accepted 2020 November 25. Received 2020 November 22; in original form 2020 October 7.

ABSTRACT

We investigate the possible origin of the transiting giant planet WD 1856+534 b, the first strong exoplanet candidate orbiting a white dwarf, through high-eccentricity migration (HEM) driven by the Lidov–Kozai (LK) effect. The host system’s overall architecture is an hierarchical quadruple in the ‘2+2’ configuration, owing to the presence of a tertiary companion system of two M-dwarfs. We show that a secular inclination resonance in 2+2 systems can significantly broaden the LK window for extreme eccentricity excitation ($e \gtrsim 0.999$), allowing the giant planet to migrate for a wide range of initial orbital inclinations. Octupole effects can also contribute to the broadening of this ‘extreme’ LK window. By requiring that perturbations from the companion stars be able to overcome short-range forces and excite the planet’s eccentricity to $e \simeq 1$, we obtain an absolute limit of $a_1 \gtrsim 8 \text{ au}$ ($a_3/1500 \text{ au}$)^{6/7} for the planet’s semi-major axis just before migration (where a_3 is the semi-major axis of the ‘outer’ orbit). We suggest that, to achieve a wide LK window through the 2+2 resonance, WD 1856 b likely migrated from $30 \text{ au} \lesssim a_1 \lesssim 60 \text{ au}$, corresponding to $\sim 10\text{--}20 \text{ au}$ during the host’s main-sequence phase. We discuss possible difficulties of all flavours of HEM affecting the occurrence rate of short-period giant planets around white dwarfs.

Key words: celestial mechanics – planets and satellites: dynamical evolution and stability – planetary systems – white dwarfs

1 INTRODUCTION

The recent discovery of WD 1856+534 b (hereafter WD 1856 b), a candidate giant planet transiting its white-dwarf (WD) host with a period of 1.4 days (Vanderburg et al. 2020), is a major milestone in the emerging field of WD planetary science. The existence of remnant planetary systems around WDs has been inferred from observations of a disintegrating planetesimal (e.g., Vanderburg et al. 2015), gas accretion from an evaporating ice giant (Gänsicke et al. 2019), infrared emission from debris discs (e.g., Farihi et al. 2009), and atmospheric pollution (Zuckerman et al. 2003, 2010; Koester et al. 2014). These phenomena are thought to be driven by tidal disruption events (Jura 2003), perhaps triggered dynamically by distant planets (Debes & Sigurdsson 2002; Debes et al. 2012; Frewen & Hansen 2014; Pichierrri et al. 2017; Mustill et al. 2018) or stellar binary partners (Bonsor & Veras 2015; Hamers & Portegies Zwart 2016b; Petrovich & Muñoz 2017; Stephan et al. 2017).

Planets orbiting within a few AU of their host stars during the main sequence are likely to be engulfed and destroyed

when the star ascends the asymptotic giant branch (AGB) on its way to becoming a WD (Villaver & Livio 2007; Mustill & Villaver 2012). The dynamical history of WD 1856b may then be similar to the hypothesized origin of hot Jupiters around main-sequence stars by high-eccentricity migration (HEM; reviewed by Dawson & Johnson 2018). During HEM, a planet’s orbital eccentricity e is excited to an extreme value ($1 - e \lesssim 10^{-2}$) via dynamical interactions. The planet then experiences strong tidal dissipation near pericenter, which shrinks and circularizes its orbit. Possible mechanisms for driving HEM are diverse, including secular interactions with other giant planets or binary companions (e.g., Wu & Murray 2003; Fabrycky & Tremaine 2007; Naoz et al. 2012; Wu & Lithwick 2011; Petrovich 2015a,b; Anderson et al. 2016; Hamers et al. 2017; Vick et al. 2019; Teyssandier et al. 2019). Similar mechanisms are plausible in a WD’s planetary system. Importantly, a successful model for the origin of WD 1856 b must be able to delay migration until the host star becomes a WD, since a planet migrating sooner than this would presumably have been destroyed.

For WD 1856 b, HEM by way of the Lidov–Kozai (LK) effect (von Zeipel 1910; Lidov 1962; Kozai 1962) is an inviting hypothesis because its host star belongs to a hierarchical

* E-mail: coconnor@astro.cornell.edu

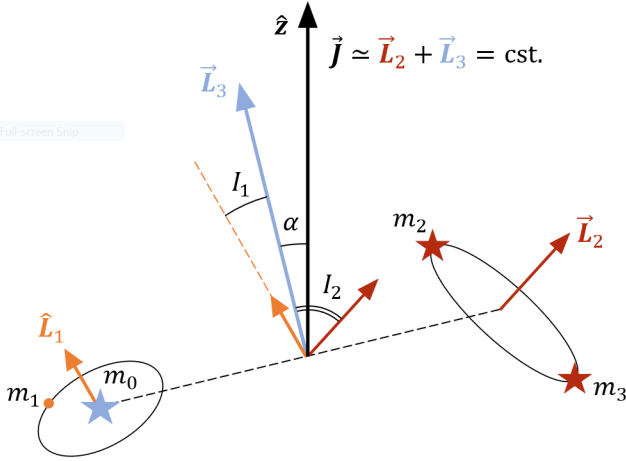


Figure 1: Schematic cartoon of a hierarchical 2+2 system with $m_1 \ll m_0, m_2, m_3$.

triple system: [Vanderburg et al. \(2020\)](#) identified two bound M-dwarf companions with a projected separation ~ 1000 au from the primary WD and ~ 50 au apart; we summarize the existing constraints on the system’s properties in Table 1. Including the planet, the system’s overall architecture is a hierarchical quadruple system with a ‘2+2’ configuration (see Figure 1). The dynamics of such systems resembles the standard LK effect in some respects but allows for the excitation of extreme eccentricities from a wider range of initial conditions ([Pejcha et al. 2013](#); [Hamers & Lai 2017](#); [Fang et al. 2018](#)).

In this paper, we demonstrate the possible origin of the WD 1856 b through HEM by way of such “enhanced” secular interactions with the WD’s stellar companions. We show that this could have occurred if the planet’s semi-major axis prior to migration was ~ 30 – 60 au, corresponding to ~ 10 – 20 au during the host’s main sequence. In Section 2, we describe the secular dynamics of a 2+2 hierarchical system and the conditions for HEM in such systems. In Section 3, we apply our dynamical model to HEM in the WD 1856 system. We examine the system’s early dynamical history in Section 4, discuss potential issues of HEM affecting the occurrence rate of giant planets around WDs in Section 5, and summarize in Section 6.

2 SECULAR DYNAMICS OF A 2+2 HIERARCHICAL SYSTEM

Figure 1 shows a schematic depiction of a 2+2 hierarchical quadruple system. The Hamiltonian describing the secular evolution of such systems has been calculated up to the quadrupole order of approximation by [Hamers et al. \(2015\)](#), [Hamers & Portegies Zwart \(2016a\)](#), and [Fang et al. \(2018\)](#). [Hamers & Lai \(2017\)](#) studied the limit where one body is a test particle and identified the key dynamical mechanism for an enhanced LK effect. We adopt their setup in this paper.

A 2+2 system can be described by three quasi-Keplerian orbits: two “inner” binary systems (labelled 1 and 2) orbit their relative barycentres, which in turn follow an “outer” orbit (3) around the system’s total centre of mass. We label the component masses m_0 and m_1

Quantity	Symbol	Value
WD mass	m_0	$0.6M_\odot$ (assumed)
Planetary mass	m_1	$1.0M_J$ (assumed)
Planetary radius	R_1	$(0.93 \pm 0.09)R_J$
Companion masses	m_2	$(0.346 \pm 0.027)M_\odot$
	m_3	$(0.331 \pm 0.024)M_\odot$
Semi-major axes	$a_{1,\text{obs}}$	≈ 0.02 au
	a_2	58^{+54}_{-16} au
	a_3	1500^{+700}_{-240} au
Eccentricities	$e_{1,\text{obs}}$	0 (assumed)
	e_2	< 0.63
	e_3	$0.30^{+0.19}_{-0.10}$

Table 1: Properties of the WD 1856 system. All values are as reported by [Vanderburg et al. \(2020\)](#) except for the WD and planetary masses, which have not been robustly measured (see Section 5.2).

for orbit 1 and m_2 and m_3 for 2. For each orbit, we denote the eccentricity vector $\mathbf{e}_k = e_k \hat{\mathbf{e}}_k$ and angular momentum vector $\mathbf{L}_k = \mu_k [GM_k a_k (1 - e_k^2)]^{1/2} \hat{\mathbf{L}}_k$, where μ_k , M_k , and a_k are respectively the reduced mass, total mass, and semi-major axis. We also define the dimensionless angular momentum $\mathbf{j}_k = (1 - e_k^2)^{1/2} \hat{\mathbf{L}}_k$ and the total angular momentum $\mathbf{J} = \mathbf{L}_1 + \mathbf{L}_2 + \mathbf{L}_3 \equiv J \hat{\mathbf{z}}$. Finally, we define $\cos I_1 = \hat{\mathbf{L}}_1 \cdot \hat{\mathbf{L}}_3$, $\cos I_2 = \hat{\mathbf{L}}_2 \cdot \hat{\mathbf{L}}_3$, and $\cos \alpha = \hat{\mathbf{L}}_3 \cdot \hat{\mathbf{z}}$ (see Fig. 1).

We consider a hierarchical system with $m_1 \ll m_{0,2,3}$ such that $L_1 \ll L_2$, $\mathbf{J} \simeq \mathbf{L}_2 + \mathbf{L}_3 = \text{const.}$, and $L_2 \sin I_2 \simeq L_3 \sin \alpha$. For simplicity, we assume that $\mathbf{e}_2 = \mathbf{0}$ and that the mutual inclination of orbits 2 and 3 is $I_2 < 39.2^\circ$ in order to suppress the LK effect for orbit 2. The latter two assumptions may not hold for general 2+2 systems, but they are appropriate for the WD 1856 system.¹

Under these assumptions, the secular evolution is completely described by the following equations:

$$\frac{d\mathbf{j}_1}{dt} = \frac{3}{4t_{\text{LK}}} \left[(\mathbf{j}_1 \cdot \hat{\mathbf{L}}_3) (\mathbf{j}_1 \times \hat{\mathbf{L}}_3) - 5 (\mathbf{e}_1 \cdot \hat{\mathbf{L}}_3) (\mathbf{e}_1 \times \hat{\mathbf{L}}_3) \right], \quad (1)$$

$$\frac{d\mathbf{e}_1}{dt} = \frac{3}{4t_{\text{LK}}} \left[(\mathbf{j}_1 \cdot \hat{\mathbf{L}}_3) (\mathbf{e}_1 \times \hat{\mathbf{L}}_3) + 2 (\mathbf{j}_1 \times \mathbf{e}_1) - 5 (\mathbf{e}_1 \cdot \hat{\mathbf{L}}_3) (\mathbf{j}_1 \times \hat{\mathbf{L}}_3) \right], \quad (2)$$

$$\frac{d\hat{\mathbf{L}}_3}{dt} = -\frac{\beta}{t_{\text{LK}}} (\hat{\mathbf{z}} \times \hat{\mathbf{L}}_3). \quad (3)$$

Above we have defined the LK time-scale for orbit 1 as

$$\frac{1}{t_{\text{LK}}} = \frac{m_{23}}{m_0} \left(\frac{a_1}{a_{3,\text{eff}}} \right)^3 n_1, \quad (4)$$

where $m_{23} = m_2 + m_3$, $a_{3,\text{eff}} = a_3(1 - e_3^2)^{1/2}$, and $n_1 = (Gm_0/a_1^3)^{1/2}$. We have also defined a dimensionless quantity

¹ For general e_2 and I_2 , the precession rate of \mathbf{L}_3 around \mathbf{J} and the angle α between \mathbf{L}_3 and \mathbf{J} both vary due to eccentricity oscillations. All these variations occur on a similar time-scale per Eq. (6). Thus we do not expect these complications to appreciably change the dynamics.

$$\beta = \frac{3}{4} \left(\frac{m_0}{m_{23}} \frac{a_2}{a_1} \right)^{3/2} \frac{J}{L_3} \cos I_2, \quad (5)$$

which is simply the precession rate of \mathbf{L}_3 about $\hat{\mathbf{z}}$,

$$\Omega_{3z} = \frac{3}{4} \frac{m_0}{m_{23}} \left(\frac{a_2}{a_{3,\text{eff}}} \right)^3 \frac{J}{L_2} n_2, \quad (6)$$

in units of t_{LK}^{-1} , i.e. $\beta = \Omega_{3z} t_{\text{LK}}$.

The qualitative nature of the dynamics is determined by the value of β (Hamers & Lai 2017). There are three regimes:

(i) When $\beta \ll 1$, $\hat{\mathbf{L}}_1$ precesses around $\hat{\mathbf{L}}_3$ more rapidly than $\hat{\mathbf{L}}_3$ around $\hat{\mathbf{z}}$. The system's dynamical evolution approaches that of a ‘2+1’ hierarchical triple in the standard LK problem. If the initial mutual inclination of orbits 1 and 3 satisfies $\cos I_{1,0} < \sqrt{3/5}$, then the eccentricity of m_1 can be excited according to

$$e_{1,\text{max}} = \sqrt{1 - \frac{5}{3} \cos^2(I_{1,0})}. \quad (7)$$

We call this the “quasi-LK” regime.

(ii) When $\beta \gg 1$, $\hat{\mathbf{L}}_1$ precesses around $\hat{\mathbf{L}}_3$ slowly compared to $\hat{\mathbf{L}}_3$ around $\hat{\mathbf{z}}$; one can then average over the precession of $\hat{\mathbf{L}}_3$, so that $\hat{\mathbf{L}}_1$ effectively precesses around $\hat{\mathbf{z}}$. The dynamics of m_1 resembles the LK problem with a modified conservation law:

$$e_{1,\text{max}} = \sqrt{1 - \frac{5}{3} \cos^2(\theta_{1,0})}, \quad (8)$$

where $\theta_{1,0}$ is the initial angle between $\hat{\mathbf{L}}_1$ and $\hat{\mathbf{z}}$. We call this the “modified LK” regime.

(iii) When $\beta \sim 1$, $\hat{\mathbf{L}}_1$ precesses around $\hat{\mathbf{L}}_3$ at roughly the same rate as $\hat{\mathbf{L}}_3$ around $\hat{\mathbf{z}}$. This secular inclination resonance drives chaotic evolution of orbit 1, featuring extreme eccentricities for a broader range of initial inclinations – an “enhanced LK window.” We call this the “resonant” regime; it is here that the quadruple nature of the system has the greatest effect.

In Figure 2, we compare the eccentricity excitation of m_1 between the modified LK and resonant regimes for trajectories with identical initial conditions. When $\beta \gg 1$, the maximal eccentricity $e_1 \approx 0.95$ is consistent with Eq. (8). When $\beta \sim 1$, however, extreme eccentricities $1 - e_1 \sim 10^{-4}$ can be achieved even with moderate initial inclinations. We quantify this in the next section.

2.1 Short-Range Forces and the ‘Extreme’ LK Window

For a planet initially at a large distance ($a_1 \gtrsim 10$ au) to migrate to ~ 0.02 au through the LK mechanism, extreme eccentricity excitation ($1 - e_1 \lesssim 10^{-3}$) is required. However, when the planet's pericenter separation $a_1(1 - e_1)$ from the host star is small, short-range forces (SRFs) can become significant. We implement these additional forces in our model following Liu et al. (2015).

We include SRFs arising from the 1PN correction to the gravitational potential of m_0 and from the tidal distortion

of m_1 . These contribute an additional term in Eq. (2):

$$\left(\frac{d\mathbf{e}_1}{dt} \right)_{\text{SRF}} = (\dot{\omega}_{1\text{PN}} + \dot{\omega}_{\text{tide}}) \hat{\mathbf{L}}_1 \times \mathbf{e}_1, \quad (9)$$

where

$$\dot{\omega}_{1\text{PN}} = \frac{3Gm_0}{c^2 a_1} \frac{n_1}{1 - e_1^2}, \quad (10)$$

$$\dot{\omega}_{\text{tide}} = \frac{15}{2} k_{2,1} \frac{m_0}{m_1} \left(\frac{R_1}{a_1} \right)^5 \frac{1 + (3/2)e_1^2 + (1/8)e_1^4}{(1 - e_1^2)^5} n_1, \quad (11)$$

with R_1 and $k_{2,1}$ the radius and tidal Love number of m_1 .

SRFs impose an upper limit e_{lim} on the eccentricity that can be achieved through secular dynamical excitation; this limit is given by (Liu et al. 2015)

$$\left(\frac{\dot{\omega}_{1\text{PN}}}{\dot{\omega}_{\text{LK}}} + \frac{1}{9} \frac{\dot{\omega}_{\text{tide}}}{\dot{\omega}_{\text{LK}}} \right)_{e_1=e_{\text{lim}}} = \frac{9}{8} \quad (12)$$

where

$$\dot{\omega}_{\text{LK}} = \frac{1}{t_{\text{LK}}(1 - e_1^2)^{1/2}}. \quad (13)$$

Eq. (12) was derived for the standard ‘2+1’ quadrupole LK problem with SRFs, but it is also valid when octupole effects are included (Liu et al. 2015; see also Section 2.2). Our numerical calculations show that it holds for the ‘2+2’ problem as well (Fig. 3).

In the general problem of HEM via the LK effect, additional SRFs can arise from the rotational distortion of m_0 and m_1 . However, rotational effects are negligible compared to the 1PN and tidal effects for a giant planet migrating around a WD (e.g., Anderson et al. 2016). The limiting eccentricity for our purposes is determined mainly by the tidal perturbation; thus:

$$\begin{aligned} 1 - e_{\text{lim}} &\simeq 5 \times 10^{-5} \left(\frac{m_0}{0.6M_\odot} \right)^{4/9} \left(\frac{m_{23}}{0.66M_\odot} \right)^{-2/9} \\ &\times \left(\frac{k_{2,1}}{0.37} \right)^{2/9} \left(\frac{R_1}{R_J} \right)^{10/9} \left(\frac{m_1}{M_J} \right)^{-2/9} \\ &\times \left(\frac{a_{3,\text{eff}}}{1500 \text{ au}} \right)^{2/3} \left(\frac{a_1}{50 \text{ au}} \right)^{-16/9}, \end{aligned} \quad (14)$$

where we have assumed planetary properties analogous to Jupiter.

To produce the observed giant planet (at $a_{1,\text{obs}} \approx 0.02$ au) around WD 1856+534 via HEM, we require the pericentre distance $a_1(1 - e_1)$ to reach below 0.01 au (recall that tidal dissipation conserves angular momentum). Using Eq. (14), we find that the semi-major axis must satisfy

$$\begin{aligned} a_1 &\gtrsim 8.4 \text{ au} \left(\frac{m_0}{0.6M_\odot} \right)^{4/7} \left(\frac{m_{23}}{0.66M_\odot} \right)^{-2/7} \\ &\times \left(\frac{k_{2,1}}{0.37} \right)^{2/7} \left(\frac{R_1}{R_J} \right)^{10/7} \left(\frac{m_1}{M_J} \right)^{-2/7} \\ &\times \left(\frac{a_{3,\text{eff}}}{1500 \text{ au}} \right)^{6/7} \left(\frac{a_{1,\text{obs}}}{0.02 \text{ au}} \right)^{-9/7}, \end{aligned} \quad (15)$$

in order for external perturbations to overcome SRFs and push the planet to sufficiently high eccentricity.

Even when Eq. (15) is satisfied, the standard ‘2+1’ LK effect can produce extreme eccentricity excitation only when $I_{1,0}$ is very close to 90 degrees (top-left panel of Fig. 3, cyan points). This is where the resonant LK effect in a 2+2 system becomes important: when $\beta \sim 1$, the inclination resonance

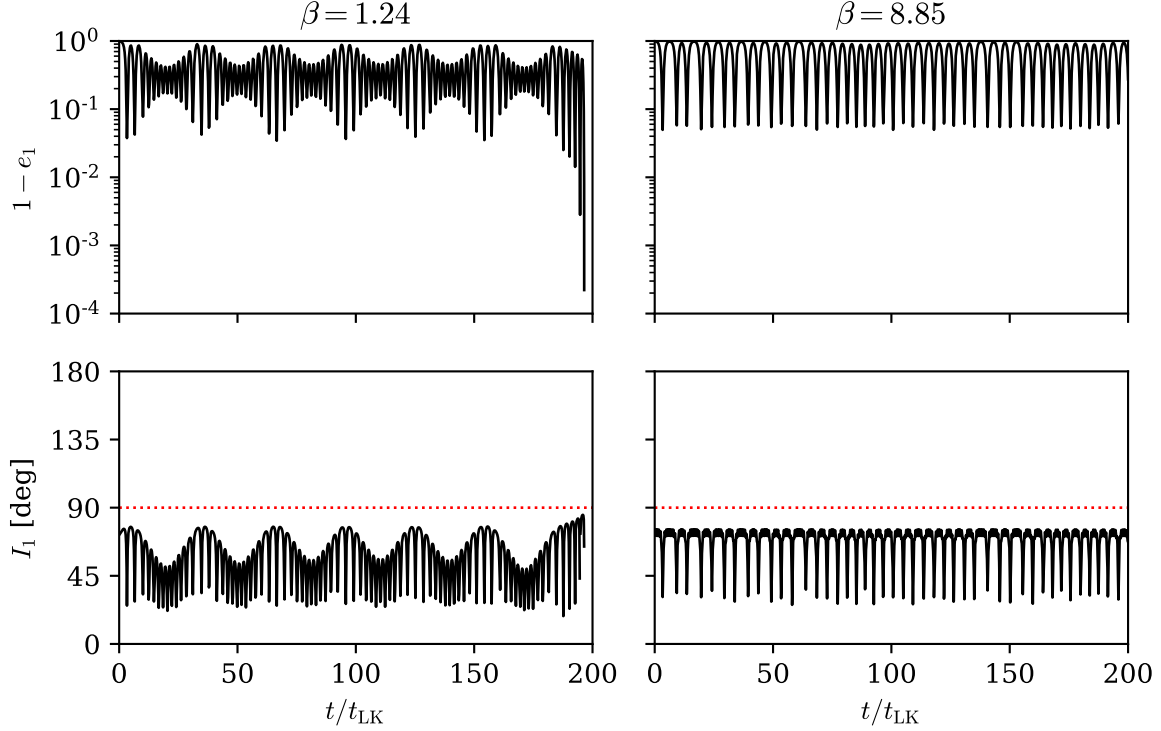


Figure 2: Eccentricity (as $1 - e_1$; upper panels) and inclination (lower) of the test particle as a function of time for trajectories in the resonant regime ($\beta \sim 1$, left panels) and modified LK ($\beta \gg 1$, right) regime. In these examples, we use identical initial conditions $I_{1,0} = 75^\circ$, $\Omega_{1,0} = 135^\circ$, $e_{1,0} = 0.01$, $\omega_{1,0} = 344^\circ$.

broadens the LK window for extreme eccentricities (Hamers & Lai 2017). For typical properties of the WD1856 system (from Table 1: $m_0 = 0.6M_\odot$, $m_2 = m_3 = 0.33M_\odot$, $a_2 = 60$ au, $a_3 = 1500$ au, $I_2 = 30^\circ$; note that $\alpha \simeq 2^\circ$ and $J \simeq L_3$), Eq. (5) provides the value of a_1 corresponding to a given β :

$$a_1 = \frac{49.5 \text{ au}}{\beta^{2/3}} \left(\frac{m_0}{0.6M_\odot} \right) \left(\frac{m_{23}}{0.66M_\odot} \right)^{-1} \times \left(\frac{a_2}{60 \text{ au}} \right) \left(\frac{\cos I_2}{\sqrt{3}/2} \right)^{2/3}. \quad (16)$$

To evaluate the ‘extreme’ LK window for a given β , we numerically integrate the quadrupole-order secular equations (including SRFs) for a duration of $500t_{\text{LK}}$ using initial conditions over the full range of $I_{1,0}$ with the angles of the node ($\Omega_{1,0}$) and pericentre ($\omega_{1,0}$) randomly distributed. Fig. 3 shows the result of this calculation as cyan points. For $\beta \ll 1$ (the quasi-LK regime), the second binary behaves like a point mass m_{23} , the relation between $I_{1,0}$ and $e_{1,\text{max}}$ is analytical (Eq. 7), and the limiting eccentricity is achieved only if the initial inclination is extremely close to 90° . For β around unity, we see a substantial widening of the extreme LK window. The window appears to be widest around $\beta = 1.5$, spanning the range $70^\circ \lesssim I_{1,0} \lesssim 110^\circ$. For progressively larger β , the window shrinks again to a narrow range around $I_{1,0} = 90^\circ$ as the system enters the modified LK regime.

Importantly, Fig. 3 confirms that despite the complex LK evolution for $\beta \sim 1$, the limiting eccentricity of Eqs. (12, 14) still sets the floor for $1 - e_1$. Note that the “double-

valued” features seen in Fig. 3 (e.g., in the lower-left panel) are a consequence of chaotic evolution for $\beta \sim 1$: the time required to achieve large eccentricities (beyond the standard ‘2+1’ LK effect) is highly variable (i.e. is sensitive to initial conditions) and may exceed $500t_{\text{LK}}$ (the duration of each integration).

2.2 Octupole-Order Effects

So far, we have discussed the dynamics of a test particle in a 2+2 system at the quadrupole order of approximation. However, octupole-order effects may be necessary for an accurate treatment for nonzero e_3 and a_1 sufficiently large. The strength of the octupole perturbation of m_1 by m_{23} relative to the quadrupole is measured by the dimensionless quantity

$$\varepsilon_{\text{oct}} = \frac{a_1}{a_3} \frac{e_3}{1 - e_3^2}. \quad (17)$$

Liu et al. (2015) showed that including the octupole terms in the 2+1 LK problem with SRFs preserves the limiting eccentricity (Eq. 12) and that octupole effects can enhance the extreme LK window. Orbit 1 can always achieve $e_1 = e_{\text{lim}}$ when the initial inclination $I_{1,0}$ exceeds a critical value $I_{1,\text{cr}}$ (i.e., $I_{1,\text{cr}} < I_{1,0} < 180^\circ - I_{1,\text{cr}}$; see the top-left panel

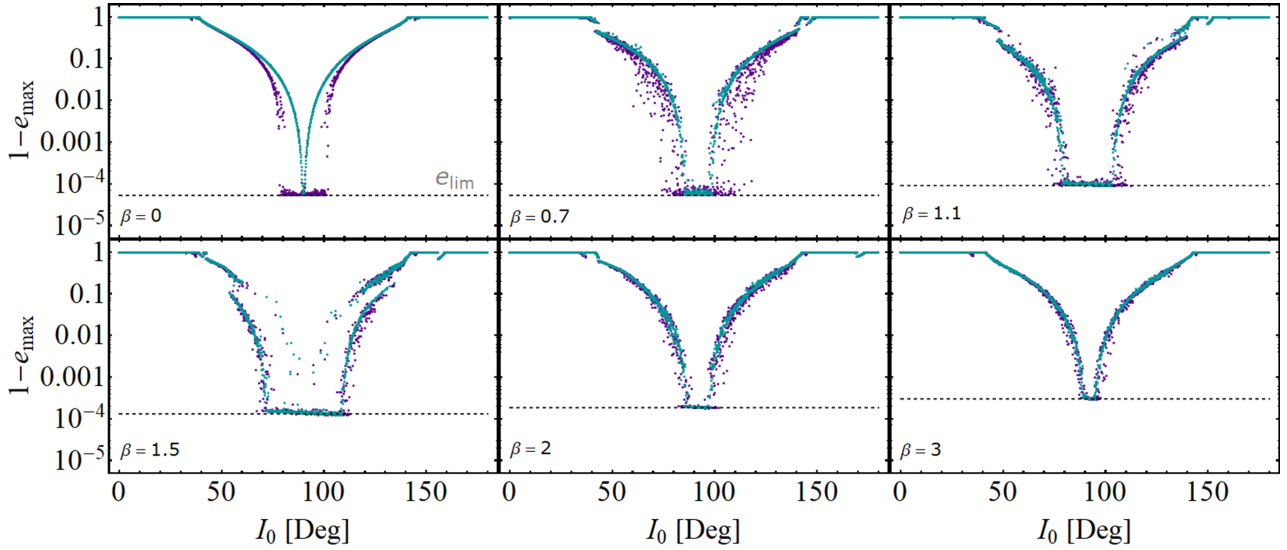


Figure 3: Maximum eccentricity of orbit 1 (as $1 - e$) versus initial inclination $I_0 \equiv I_{1,0}$ for different values of β (Eq. 5). In all cases, we choose $m_0 = 0.6M_\odot$, $m_1 = 1.0M_J$, $m_2 = m_3 = 0.33M_\odot$, $a_2 = 60$ au (except the top-left panel where $a_2 = 1$ au), $e_2 = 0$, $e_3 = 0.3$, $a_3 = 1500$ au, and $I_2 = 30^\circ$ ($\alpha \approx 2^\circ$). The value of a_1 in each panel is 52 au ($\beta = 0$ and $\beta = 0.7$), 38.5 au ($\beta = 1.1$), 31.3 au ($\beta = 1.5$), 25.8 au ($\beta = 2$), and 19.7 au ($\beta = 3$). The planet’s initial $e_{1,0} = 0.01$. The argument of pericentre $\omega_{1,0}$ and longitude of the node $\Omega_{1,0}$ are randomly chosen in $[0, 2\pi)$. We integrate the vectorial secular equations for $500t_{LK}$ and plot the maximal eccentricity achieved by m_1 in that time. We include SRFs due to the 1PN correction and tidal distortion of m_1 , assuming $R_1 = 1.0R_J$ and $k_{2,1} = 0.37$. The cyan dots represent the results including quadrupole-order perturbations and SRFs whilst the purple dots also include the octupole-order terms from m_{23} perturbing m_1 . The dotted horizontal line is the limiting eccentricity e_{lim} of Eq. (12).

of Fig. 3). An analytical fit for $I_{1,cr}$ is

$$\cos^2(I_{1,cr}) \simeq 0.26 \left(\frac{\varepsilon_{oct}}{0.1} \right) - 0.536 \left(\frac{\varepsilon_{oct}}{0.1} \right)^2 + 12.05 \left(\frac{\varepsilon_{oct}}{0.1} \right)^3 - 16.78 \left(\frac{\varepsilon_{oct}}{0.1} \right)^4 \quad (18)$$

for $\varepsilon_{oct} \lesssim 0.05$ and $\cos^2(I_{1,cr}) \simeq 0.45$ for $\varepsilon_{oct} \gtrsim 0.05$ (Muñoz et al. 2016). This form of enhancement is independent of the secular resonance effect in a 2+2 system and therefore can persist when $\beta \ll 1$. For fiducial properties of the WD 1856 system ($a_3 = 1500$ au, $e_3 = 0.3$), we have

$$\varepsilon_{oct} \simeq 0.01 \left(\frac{30a_1}{a_3} \right) \left(\frac{e_3}{0.3(1 - e_3^2)} \right), \quad (19)$$

$$|I_{1,cr} - 90^\circ| \simeq 10^\circ \left(\frac{30a_1}{a_3} \right)^{1/2} \left(\frac{e_3}{0.3(1 - e_3^2)} \right)^{1/2}. \quad (20)$$

In order to evaluate the relative contributions of the octupole and 2+2 “resonant” effects to the enhancement of LK window, we repeat the exercise of Section 2.1, this time including additional terms in Eqs. (1)–(3) to describe the octupole-order perturbation of orbit 1 by orbit 3 following Liu et al. (2015) (see also Liu & Lai 2019). The results are displayed as purple points in Fig. 3. As predicted, the octupole-order results feature an extreme LK window even for $\beta \ll 1$, consistent with Eq. (20).

For $\beta = 0.7$, the inclusion of octupole effects significantly widens the LK window relative to 2+2 resonant quadrupole effects alone. This suggests that the resonant-quadrupole and octupole effects can interfere constructively for $0.1 \lesssim \beta \lesssim 1$. For $\beta \gtrsim 1$, a_1 and ε_{oct} are smaller and the “resonant” quadrupole effect dominates the width of the extreme LK window; in these cases, octupole effects introduce

a modest scatter in $e_{1,max}$ about the quadrupole result but do not otherwise affect the outcome.

3 HIGH-ECCENTRICITY MIGRATION AROUND WD 1856+534

We now apply our model to the WD 1856+534 system in order to demonstrate the feasibility of HEM through the enhanced LK effect in the resonant regime. For simplicity, we do not simulate the system’s dynamical evolution prior to the WD phase (but see Section 4). We also neglect octupole effects in this section.

We assume the same stellar and planetary parameters as in the previous section. In addition to the quadrupole secular perturbations and SRFs used previously, we now include dissipation of the equilibrium tide raised on the planet by the WD. We adopt the weak-friction model, where the planet’s internal dissipation is parametrized by a constant lag-time $\Delta t_{L,1}$ (e.g., Alexander 1973; Hut 1981). The additional terms in Eqs. (1, 2) due to weak friction are given by Anderson et al. (2016). We assume that the planet rotates pseudosynchronously during HEM.

In Figure 4, we display an example of successful HEM of WD 1856 b from an initial configuration with $a_1 = 40$ au (corresponding to $\beta = 1.11$) and $I_1 = 75^\circ$. For this example, we adopt $\Delta t_{L,1} = 10$ s, corresponding to a factor of 100 enhancement relative to Jupiter’s dissipation; this is necessary to ensure timely orbital circularization of the planet and avoid tidal disruption (see Section 5). The planet’s minimal pericentre distance is just larger than the tidal disruption

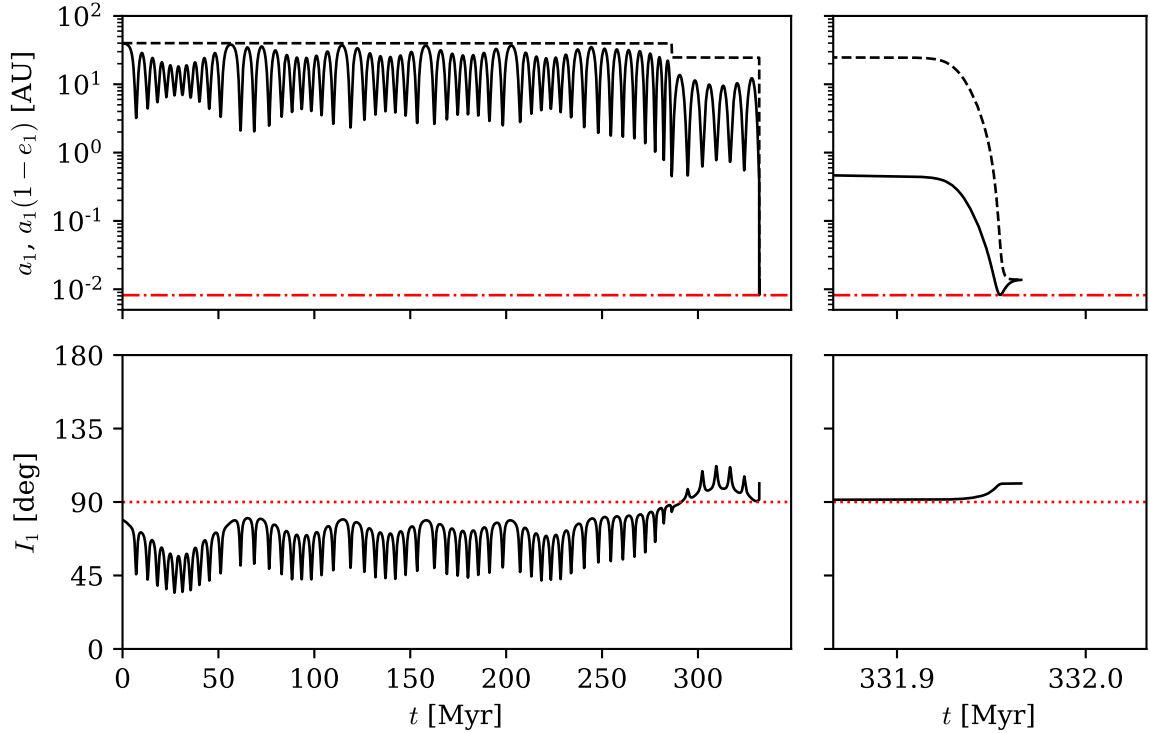


Figure 4: An example of HEM of a Jupiter-like planet in the WD 1856 system through the resonant ‘2+2’ LK effect. The upper panels show the semi-major axis (a_1 , dashed black curve) and pericentre distance ($a_1[1 - e_1]$, solid black) with the tidal disruption radius $\approx 2R_1(m_0/m_1)^{1/3}$ (horizontal red line) marked for reference. The lower panels show the inclination I_1 (black curve) with $I_1 = 90^\circ$ (in red) for reference. The left panels show the full integration over ~ 332 Myr whilst the right panels zoom in on the final circularization phase. The parameters are: WD mass $m_0 = 0.6M_\odot$, planetary mass and radius $m_1 = 1.0M_J$ and $R_1 = 1.0R_J$, companion masses $m_2 = m_3 = 0.33M_\odot$, $a_2 = 60$ au, $a_3 = 1500$ au, $e_3 = 0.3$, and $I_2 = 30^\circ$, corresponding to $\alpha \approx 2^\circ$ and $\beta = 1.11$. The planet’s initial conditions are $a_1 = 40$ au, $e_1 = 0.01$, $I_1 = 75^\circ$, $\Omega_1 = 289^\circ.7$, and $\omega_1 = 175^\circ.4$, and the tidal Love number and lag-time are $k_{2,1} = 0.37$ and $\Delta t_{L,1} = 10$ s. Note that the planet’s final orbit is retrograde and nearly perpendicular to orbit 3.

limit,

$$r_{p,\text{dis}} = \eta R_1 \left(\frac{m_0}{m_1} \right)^{1/3} \quad (21)$$

where $\eta \approx 2\text{--}3$ for a giant planet (e.g., [Guillochon et al. 2011](#)). The planet’s final semi-major axis is approximately twice this value, close to WD 1856 b’s orbit at ≈ 0.02 au. The entire evolution takes place in slightly less than 332 Myr, well within the ~ 6 Gyr cooling age of WD 1856 ([Vanderburg et al. 2020](#)).

We note in the bottom panels of Fig. 4 that the planet’s final orbit is nearly perpendicular to the outer orbit. This is consistent with the actual viewing geometry for this system, with orbit 3 lying roughly in the celestial plane and orbit 1 along the line of sight ([Vanderburg et al. 2020](#)).

4 PRE-WD DYNAMICAL EVOLUTION

Let us consider the possible dynamical evolution of the WD 1856 system prior to the WD phase. As we noted previously, the transiting planet could not have migrated to its current location until after the host star had evolved into a

WD; if an enhanced LK effect was responsible for this migration, then it is desirable that the effect be suppressed prior to the WD phase. The two most likely ways to accomplish this involve stellar evolution or the presence of additional planets in this system prior to the WD phase.

Most known WDs that show evidence for planetary systems evolved from main-sequence (MS) stars somewhat more massive than the Sun, typically $\sim 1.5\text{--}3.0M_\odot$ ([Koester et al. 2014](#)). Such stars become WDs of $\sim 0.5\text{--}0.8M_\odot$ ([Kalirai et al. 2008](#); [Choi et al. 2016](#)), losing most of their mass during the AGB phase. AGB mass loss occurs over several Myr, a long time-scale compared to the orbital period of planetary or stellar companions closer than $\sim 10^4$ au; thus its effect on a 2+2 system can be treated using the principle of adiabatic invariance.

Consider the adiabatic reduction of the primary mass from $m_{0,\text{MS}}$ (the MS value) to $m_0 = fm_{0,\text{MS}}$ (the final WD mass, with $f < 1$). Assuming that mass is expelled isotropically and that none is captured by the other bodies, adiabatic invariance implies that orbits 1 and 3 expand according

to

$$a_{1,\text{MS}} \rightarrow a_1 = \frac{a_{1,\text{MS}}}{f}, \quad (22)$$

$$a_{3,\text{MS}} \rightarrow a_3 = \frac{m_{0,\text{MS}} + m_{23}}{m_0 + m_{23}} a_{3,\text{MS}} \quad (23)$$

whilst all other orbital elements are unchanged. It follows that the LK time-scale and the parameter β change according to

$$t_{\text{LK,MS}} \rightarrow t_{\text{LK}} = f^2 \left(\frac{m_{0,\text{MS}} + m_{23}}{m_0 + m_{23}} \right)^3 t_{\text{LK,MS}}, \quad (24)$$

$$\beta_{\text{MS}} \rightarrow \beta = f^3 \beta_{\text{MS}}, \quad (25)$$

where we have used $J \simeq L_3$ and $I_2 = \text{constant}$ during the evolution. We see that adiabatic mass loss reduces β by a large factor. Thus, orbit 1 can transition from the modified LK regime ($\beta_{\text{MS}} \gg 1$) to the resonant regime ($\beta \sim 1$) as a result of stellar mass loss.

For typical WD 1856 system parameters, significant enhancement of the extreme LK window requires $2 \gtrsim \beta \gtrsim 0.7$ (Fig. 3), corresponding to the planet's semi-major axis at the end of the AGB phase in the range $28 \text{ au} \lesssim a_1 \lesssim 57 \text{ au}$ (Eq. 16). If we adopt $m_0 = 0.6 M_\odot$ for the WD and $m_{0,\text{MS}} = 2.0 M_\odot$ for the progenitor (per the initial-final mass relation of Kalirai et al. 2008), i.e. $f = 0.3$, we find that this “resonant” a_1 range translates to $8 \text{ au} \lesssim a_{1,\text{MS}} \lesssim 17 \text{ au}$. This is consistent with WD 1856 b having been a typical “cold Jupiter” during the MS.

As discussed in Section 2.2, octupole-order effects can also enhance the window for extreme eccentricity excitation through the LK effect. During adiabatic mass loss, ε_{oct} (Eq. 17) evolves according to

$$\varepsilon_{\text{oct,MS}} \rightarrow \varepsilon_{\text{oct}} = \frac{1}{f} \left(\frac{m_0 + m_{23}}{m_{0,\text{MS}} + m_{23}} \right) \varepsilon_{\text{oct,MS}}. \quad (26)$$

For the canonical masses in the WD 1856 system and $f = 0.3$, we have $\varepsilon_{\text{oct,MS}} \approx 0.63 \varepsilon_{\text{oct}}$, meaning octupole effects are less important during the MS (see also Stephan, Naoz & Gaudi 2020). From Eqs. (19, 20), octupole effects can induce an appreciable extreme LK window (e.g., wider than 10°) only if the planet's semi-major axis is larger than $\sim 1/30$ of the semi-major axis of orbit 3, or $a_{1,\text{MS}} \gtrsim 24 \text{ au}$ for $a_{3,\text{MS}} = 700 \text{ au}$.

In principle, HEM through the LK effect could occur during the MS. Equation (14) with the above MS system parameters implies that a planet at $a_{1,\text{MS}} \approx 15 \text{ au}$ could have reached a pericentre distance $a_{1,\text{MS}}(1 - e_{\text{lim}}) \approx 0.007 \text{ au}$. However, the inclination window to reach such extreme eccentricities would have been narrow since $\beta_{\text{MS}} \gg 1$ and $\varepsilon_{\text{oct,MS}} \ll 1$. AGB mass loss expands the extreme LK window, acting as a “trigger” for HEM during the WD phase.

In addition to the effects of stellar evolution, another planet orbiting closer to the host star could have suppressed the LK effect during the MS by augmenting the free precession rate of WD 1856 b (see Holman et al. 1997; Petrovich & Muñoz 2017). A planet of mass m' at a distance $a' < a_{1,\text{MS}}$ from the host star would completely suppress LK oscillations of m_1 if

$$\begin{aligned} m' &\gtrsim m_{23} \frac{a_{1,\text{MS}}^5}{a_{3,\text{MS}}^3 (a')^2} \\ &\approx 0.2 M_J \left(\frac{a_{1,\text{MS}}}{10 \text{ au}} \right)^5 \left(\frac{a_{3,\text{MS}}}{700 \text{ au}} \right)^{-3} \left(\frac{a'}{1 \text{ au}} \right)^{-2}. \end{aligned} \quad (27)$$

A smaller m' would still be sufficient to suppress high-eccentricity excursions of m_1 . If this planet had $a' \lesssim 3 \text{ au}$ during the MS, it would have been engulfed during the AGB stage (e.g., Mustill & Villaver 2012), thereby “switching on” the LK effect during the WD phase. The architecture envisioned in this scenario (i.e., two planets between ~ 1 and 20 au) is plausible given current knowledge of the population of extrasolar planets. For instance, Bryan et al. (2016) found that $\sim 50\%$ of giant planets orbiting between 1 and 5 au have companions of comparable mass within a distance of 20 au .

5 MAIN CAVEATS AND UNCERTAINTIES

5.1 Tidal Disruption and Survival of Migrating Planets

The challenges of HEM through secular dynamics have been studied in the context of hot-Jupiter formation around MS stars. A major issue is that it is easy for a migrating planet to be tidally disrupted. Population-synthesis models (Petrovich 2015a; Anderson et al. 2016; Hamers et al. 2017; Vick et al. 2019; Teyssandier et al. 2019) and analytical calculations (Muñoz et al. 2016) show that tidal disruption can limit the efficiency of hot-Jupiter formation through secular HEM to a few percent. In particular, although octupole effects broaden the ‘extreme’ LK window and thus increase the migration fraction, most migrating planets are tidally disrupted (Anderson et al. 2016; Muñoz et al. 2016). A similar situation occurs for the secular-chaos scenario (Wu & Lithwick 2011; Teyssandier et al. 2019). In Section 3, although we have not systematically surveyed a large parameter space, we also find that a large fraction of migrating planets are disrupted for HEM in 2+2 systems. In fact, we had to use a relatively large tidal lag-time ($\Delta t_{\text{L},1} = 10 \text{ s}$) in order to find a reasonable number of surviving cases.

The problem of tidal disruption during HEM can be somewhat alleviated by invoking forms of tidal dissipation other than weak friction, such as chaotic dynamical tides with non-linear dissipation (Vick & Lai 2018; Wu 2018; Vick et al. 2019; Teyssandier et al. 2019; Veras & Fuller 2019). Vick et al. (2019) show that the strong dissipation associated with chaotic tides can shepherd to safety some planets that are otherwise destined for tidal disruption by rapidly decreasing their eccentricities; they find $\sim 20\%$ of migrating planets survive with short final orbital periods.

Strong planet-planet scattering may also give rise to HEM. A planetary system that is dynamically stable during the MS can become unstable after AGB stellar mass loss (Debes & Sigurdsson 2002). However, strong scattering of unstable giant planets mostly results in ejections or planetary mergers. The ‘branching ratio’ of one planet being injected into a low-pericentre orbit suitable for HEM is small (e.g., Mustill et al. 2014; Veras & Gänsicke 2015; Veras et al. 2016; Anderson et al. 2020; Li et al. 2021) unless the initial number of unstable planets is large (Maldonado et al. 2021). We therefore consider this a less promising HEM mechanism.

5.2 Properties of WD and Planet

We have assumed fiducial masses of $m_0 = 0.6M_\odot$ and $m_1 = 1.0M_J$ for the WD and planet, respectively. [Vanderburg et al. \(2020\)](#) report a somewhat smaller WD mass of $(0.52 \pm 0.06)M_\odot$ and obtain only an upper bound of $13.8M_J$ for the planet. The exact masses one assumes do not affect the key conclusions of this work as far as the LK effect is concerned. Since WD 1856 b has at most $\sim 2\%$ the mass of its host, the test-particle approximation is reasonable. Decreasing m_0 or increasing m_1 weakly affects the limiting eccentricity (Eq. 14), shifting the minimal a_1 for migration (Eq. 15), and the tidal disruption distance (Eq. 21) slightly inward. The range of a_1 for which the 2+2 resonance is active also shifts slightly inward for decreased m_0 (Eq. 16). The tidal circularization timescale, which is proportional to $m_1/(m_0)^2$ in the weak-friction theory, is affected more significantly. If the planet's true mass is $10M_J$, then stronger dissipation ($\Delta t_{L,1} \gtrsim 10^2$ s) would be required for the planet's migration and survival (but see Section 5.1 for a discussion of chaotic dynamical tides).

The values of the mass and cooling age of WD 1856 reported by [Vanderburg et al. \(2020\)](#) were obtained by fitting atmospheric models to the stellar spectrum. Taken at face value, the best-fitting model – with a WD mass of $0.52M_\odot$ and a cooling age of ~ 6 Gyr – implies a roughly solar-mass progenitor that spent ~ 10 Gyr on the MS. However, this is at odds with the system's likely membership in the Galactic thin disc, which would imply that the system is younger than ~ 10 Gyr in total. [Lagos et al. \(2021\)](#) have suggested a resolution to this conundrum in which WD 1856 b migrated through common-envelope evolution, reducing the final mass of the WD relative to its progenitor in the process (see also [Livio & Soker 1984](#)). On the other hand, a modest systematic error in the estimated WD mass, perhaps due to the difficulty of fitting WD 1856's featureless spectrum, can also eliminate the age discrepancy without invoking common-envelope evolution ([Vanderburg et al. 2020](#)). Our assumption about the WD and progenitor masses aligns with the latter explanation.

5.3 Occurrence Rates

The observed configuration of WD 1856 b is improbable: the planet only obscures half of the WD in transit despite having ~ 10 times its radius ([Vanderburg et al. 2020](#)). The probability of observing such 'grazing' transits is $\sim R_0/a_{1,\text{obs}} = 0.2\%$ (for $a_{1,\text{obs}} = 0.02$ au and WD radius $R_0 \approx R_\oplus$) whilst the probability of a 'full' transit is $\sim R_J/a_{1,\text{obs}} = 2\%$. Hence, the detection of WD 1856 b with a 'grazing' transit suggests there could be ~ 10 times as many systems where the WD is completely blocked. However, no other transit of a WD by a giant planet has been detected by TESS thus far, suggesting that the transit geometry of WD 1856 b is "lucky" (A. Vanderburg, private communication). Given that TESS has observed ~ 1700 isolated WDs thus far ([Vanderburg et al. 2020](#)), this would imply that short-period giant planets could orbit $\sim 2\text{--}3\%$ of them. This agrees with the 2σ upper limit obtained from the WD sample observed by *Kepler*/K2 ([van Sluijs & Van Eylen 2018](#)) but is somewhat higher than that from Pan-STARRS ([Fulton et al. 2014](#)). The discovery of additional planets transiting WDs will eventually allow

an assessment of whether this population can be attributed to HEM alone.

6 CONCLUSION

In this paper, we have demonstrated the possible HEM of WD 1856 b through an enhanced LK effect from the WD's distant M-dwarf companions. We show that the inclination resonance in hierarchical 2+2 systems and the octupole effect can both significantly broaden the LK window for extreme eccentricity excitation (see Fig. 3), allowing HEM to operate in the WD 1856 system for a wide range of initial planetary orbital inclinations. The requirement that secular perturbations from the companion stars be able to overcome SRFs imposes an absolute limit of $a_1 \gtrsim 8$ au for the planet's semi-major axis just prior to migration. Due to the large enhancement of the extreme LK window by the 2+2 resonance, we find that the planet most likely migrated from $30 \text{ au} \lesssim a_1 \lesssim 60 \text{ au}$, corresponding to $\sim 10\text{--}20$ au during the host's MS phase. Importantly, extreme eccentricity excitation through the 2+2 resonance is delayed until the WD phase at this distance.

Although WD 1856 b is so far the only intact short-period giant planet known to orbit a WD, HEM and tidal disruption of giant planets may have occurred in other WD systems. For instance, WD J0914+1914 possesses a gaseous accretion disc and a pollution signature rich in hydrogen, oxygen, and sulfur ([Gänsicke et al. 2019](#)). This has been interpreted as evidence for an ice giant's ongoing or previous disruption by the WD. As noted in Section 5, any flavor of HEM will more likely lead to tidal disruption than survival of the planet. Although WD J0914+1914's cooling age is quite short (~ 13 Myr), secular interactions can deliver a planet to the WD in time given a suitable companion ([Stephan et al. 2020](#)).

Atmospheric pollution may be a more prevalent signature of remnant planetary systems around WDs than the occurrence of short-period giant planets. To advance understanding of the occurrence of planetary systems in multiple-star systems, we recommend further observational efforts to determine the fraction of polluted WDs that belong to wide binaries or hierarchical triples. Previous studies by [Zuckerman \(2014\)](#) and [Wilson et al. \(2019\)](#) find consistent pollution fractions among WDs occurring singly and in wide binaries. The *Gaia* mission and LSST will aid in the identification of previously unknown stellar or substellar companions of WDs (e.g., [Gentile Fusillo et al. 2019](#)), offering the opportunity to refine these results.

After the original submission of this work, other studies of LK migration of WD 1856 b were independently put forth ([Muñoz & Petrovich 2020](#); [Stephan et al. 2020](#)). These works did not consider the full '2+2' LK effect but rather focused on the '2+1' octupole effect (see Section 2.2). [Muñoz & Petrovich \(2020\)](#) argue for an initial semi-major axis $a_{1,\text{MS}} \sim 2\text{--}3$ au (or $a_1 \sim 6\text{--}10$ au just before migration), as a planet with greater a_1 would experience a stronger octupole LK effect and therefore might be tidally disrupted (assuming the weak-friction tidal theory). However, migration from $a_1 \lesssim 10$ au can occur only when the initial inclination is close to 90° (Eq. 18), which is relatively unlikely. The problem of tidal disruption may be alleviated by chaotic tides

(see Section 5.1). Meanwhile, Stephan et al. (2020) favour an initial orbit $20 \text{ au} \lesssim a_{1,\text{MS}} \lesssim 100 \text{ au}$, for which the 2+1 octupole effect can excite extreme eccentricities for a wide range of inclinations. Since they did not account for the resonant effect in 2+2 systems, one would not expect planets to migrate from $a_{1,\text{MS}} \lesssim 20 \text{ au}$ in their calculations. Planets on such large orbits may also experience a strong octupole effect during the MS, depending on their initial inclination; the range of inclinations in which octupole-driven HEM is *forbidden* during the host's MS phase but *possible* during the WD phase is somewhat narrow. Finally, we note that there is some evidence that the giant-planet occurrence rate declines for $a_{1,\text{MS}} \gtrsim 20 \text{ au}$ (e.g. Bryan et al. 2016; Vigan et al. 2017).

ACKNOWLEDGEMENTS

CEO thanks Alexander Stephan, Dimitri Veras, and Laetitia Rodet for helpful discussions and the anonymous referee for comments on the manuscript. This work has been supported in part by National Science Foundation grant AST-1715246. This research has made use of NASA's Astrophysics Data System and of the software packages MATPLOTLIB (Hunter 2007), NUMPY (van der Walt et al. 2011), and SCIPY (Virtanen et al. 2020).

DATA AVAILABILITY

The data underlying this article will be shared on reasonable request to the corresponding author.

REFERENCES

Alexander M. E., 1973, *Ap&SS*, **23**, 459
 Anderson K. R., Storch N. I., Lai D., 2016, *MNRAS*, **456**, 3671
 Anderson K. R., Lai D., Pu B., 2020, *MNRAS*, **491**, 1369
 Bonsor A., Veras D., 2015, *MNRAS*, **454**, 53
 Bryan M. L., et al., 2016, *ApJ*, **821**, 89
 Choi J., Dotter A., Conroy C., Cantiello M., Paxton B., Johnson B. D., 2016, *ApJ*, **823**, 102
 Dawson R. I., Johnson J. A., 2018, *ARA&A*, **56**, 175
 Debes J. H., Sigurdsson S., 2002, *ApJ*, **572**, 556
 Debes J. H., Walsh K. J., Stark C., 2012, *ApJ*, **747**, 148
 Fabrycky D., Tremaine S., 2007, *ApJ*, **669**, 1298
 Fang X., Thompson T. A., Hirata C. M., 2018, *MNRAS*, **476**, 4234
 Farihi J., Jura M., Zuckerman B., 2009, *ApJ*, **694**, 805
 Frewen S. F. N., Hansen B. M. S., 2014, *MNRAS*, **439**, 2442
 Fulton B. J., et al., 2014, *ApJ*, **796**, 114
 Gänsicke B. T., Schreiber M. R., Toloza O., Fusillo N. P. G., Koester D., Manser C. J., 2019, *Nature*, **576**, 61
 Gentile Fusillo N. P., et al., 2019, *MNRAS*, **482**, 4570
 Guillochon J., Ramirez-Ruiz E., Lin D., 2011, *ApJ*, **732**, 74
 Hamers A. S., Lai D., 2017, *MNRAS*, **470**, 1657
 Hamers A. S., Portegies Zwart S. F., 2016a, *MNRAS*, **459**, 2827
 Hamers A. S., Portegies Zwart S. F., 2016b, *MNRAS*, **462**, L84
 Hamers A. S., Perets H. B., Antonini F., Portegies Zwart S. F., 2015, *MNRAS*, **449**, 4221
 Hamers A. S., Antonini F., Lithwick Y., Perets H. B., Portegies Zwart S. F., 2017, *MNRAS*, **464**, 688
 Holman M., Touma J., Tremaine S., 1997, *Nature*, **386**, 254
 Hunter J. D., 2007, *Computing in Science and Engineering*, **9**, 90

Hut P., 1981, *A&A*, **99**, 126
 Jura M., 2003, *ApJ*, **584**, L91
 Kalirai J. S., Hansen B. M. S., Kelson D. D., Reitzel D. B., Rich R. M., Richer H. B., 2008, *ApJ*, **676**, 594
 Koester D., Gänsicke B. T., Farihi J., 2014, *A&A*, **566**, A34
 Kozai Y., 1962, *AJ*, **67**, 591
 Lagos F., Schreiber M. R., Zorotovic M., Gänsicke B. T., Ronco M. P., Hamers A. S., 2021, *MNRAS*, **501**, 676
 Li J., Lai D., Anderson K. R., Pu B., 2021, *MNRAS*, **501**, 1621
 Lidov M. L., 1962, *Planet. Space Sci.*, **9**, 719
 Liu B., Lai D., 2019, *MNRAS*, **483**, 4060
 Liu B., Muñoz D. J., Lai D., 2015, *MNRAS*, **447**, 747
 Livio M., Soker N., 1984, *MNRAS*, **208**, 763
 Maldonado R. F., Villaver E., Mustill A. J., Chávez M., Bertone E., 2021, *MNRAS*, **501**, L43
 Muñoz D. J., Petrovich C., 2020, *ApJ*, **904**, L3
 Muñoz D. J., Lai D., Liu B., 2016, *MNRAS*, **460**, 1086
 Mustill A. J., Villaver E., 2012, *ApJ*, **761**, 121
 Mustill A. J., Veras D., Villaver E., 2014, *MNRAS*, **437**, 1404
 Mustill A. J., Villaver E., Veras D., Gänsicke B. T., Bonsor A., 2018, *MNRAS*, **476**, 3939
 Naoz S., Farr W. M., Rasio F. A., 2012, *ApJ*, **754**, L36
 Pejcha O., Antognini J. M., Shappee B. J., Thompson T. A., 2013, *MNRAS*, **435**, 943
 Petrovich C., 2015a, *ApJ*, **799**, 27
 Petrovich C., 2015b, *ApJ*, **805**, 75
 Petrovich C., Muñoz D. J., 2017, *ApJ*, **834**, 116
 Pichierri G., Morbidelli A., Lai D., 2017, *A&A*, **605**, A23
 Stephan A. P., Naoz S., Zuckerman B., 2017, *ApJ*, **844**, L16
 Stephan A. P., Naoz S., Gaudi B. S., 2020, arXiv e-prints, p. arXiv:2010.10534
 Teyssandier J., Lai D., Vick M., 2019, *MNRAS*, **486**, 2265
 Vanderburg A., et al., 2015, *Nature*, **526**, 546
 Vanderburg A., et al., 2020, *Nature*, **585**, 363
 Veras D., Fuller J., 2019, *MNRAS*, **489**, 2941
 Veras D., Gänsicke B. T., 2015, *MNRAS*, **447**, 1049
 Veras D., Mustill A. J., Gänsicke B. T., Redfield S., Georgakarakos N., Bowler A. B., Lloyd M. J. S., 2016, *MNRAS*, **458**, 3942
 Vick M., Lai D., 2018, *MNRAS*, **476**, 482
 Vick M., Lai D., Anderson K. R., 2019, *MNRAS*, **484**, 5645
 Vigan A., et al., 2017, *A&A*, **603**, A3
 Villaver E., Livio M., 2007, *ApJ*, **661**, 1192
 Virtanen P., et al., 2020, *Nature Methods*, **17**, 261
 Wilson T. G., Farihi J., Gänsicke B. T., Swan A., 2019, *MNRAS*, **487**, 133
 Wu Y., 2018, *AJ*, **155**, 118
 Wu Y., Lithwick Y., 2011, *ApJ*, **735**, 109
 Wu Y., Murray N., 2003, *ApJ*, **589**, 605
 Zuckerman B., 2014, *ApJ*, **791**, L27
 Zuckerman B., Koester D., Reid I. N., Hünsch M., 2003, *ApJ*, **596**, 477
 Zuckerman B., Melis C., Klein B., Koester D., Jura M., 2010, *ApJ*, **722**, 725
 van Sluijs L., Van Eylen V., 2018, *MNRAS*, **474**, 4603
 van der Walt S., Colbert S. C., Varoquaux G., 2011, *Computing in Science and Engineering*, **13**, 22
 von Zeipel H., 1910, *Astronomische Nachrichten*, **183**, 345